The origin of placental mammal life histories

Gregory F. Funston[1*], Paige E. dePolo[1], Jakub T. Sliwinski[2], Matthew Dumont[2], Sarah L. Shelley[1], Laetitia E. Pichevin[1], Nicola J. Cayzer[1], John R. Wible[3], Thomas E. Williamson[4], James W. B. Rae[2], Stephen L. Brusatte[1*]

[1] School of GeoSciences, University of Edinburgh, Edinburgh, UK

[2] School of Earth and Environmental Sciences, University of St. Andrews, St. Andrews, UK

[3] Carnegie Museum of Natural History, Pittsburgh, Pennsylvania, USA

[4] New Mexico Museum of Natural History and Science, Albuquerque, New Mexico, USA

*Correspondence to: Gregory.Funston@ed.ac.uk or Stephen.Brusatte@ed.ac.uk

After the end-Cretaceous extinction, placental mammals quickly diversified[1], occupied key ecological niches[2,3], and increased in size[4,5], but the latter was not true of other therians[6]. The uniquely extended gestation of placental young[7] may have factored in their success and size increase[8], but reproduction style in early placentals remains unknown. Here, using palaeohistology and geochemistry, we present the earliest record of a placental life history, in a 62-million year old pantodont, the clade including the first mammals to achieve truly large body sizes. We extend the application of dental trace element mapping[9,10] by sixty million years, identifying chemical markers of birth and weaning, and calibrate these to a daily record of growth in the dentition. A long gestation (~7 months), rapid dental development, and short suckling interval (~30–75 days) show *Pantolambda bathmodon* was highly precocial, unlike non-placental mammals and known Mesozoic precursors. These results demonstrate *P. bathmodon* reproduced like a placental, and lived at a fast pace for its body size. Assuming *P. bathmodon* reflects close placental relatives, our findings suggest the ability to produce well-developed precocial young was established early in placental evolution, and that larger neonate sizes were a possible mechanism for rapid size increase in early placentals.

Placentals are the most diverse group of mammals, comprising >6,000 extant species[11] and the largest animals ever. Their success may relate to their derived life history[8,12], with maternal investment shifted prenatally through extended gestation[7,13]. This adaptation allows placentals the unique capability among mammals to produce highly precocial young: typically single offspring born at larger masses with well-developed dentition, fur, and open eyes[13,14]. Extended

gestation may have released placentals from developmental constraints associated with prolonged lactation in other mammals[8,15,16], enabling experimentation with new locomotor modes and habitats[17,18]. However, when extended gestation evolved in mammals remains unclear: Mesozoic eutherians (mammals more closely related to placentals than marsupials) did not grow like living placentals[19–21] and it has been hypothesized that ancestral placentals gave birth to altricial young[21]. Nonetheless, immediately after the end-Cretaceous extinction, early Palaeocene placentals emerged from a 100-Ma lineage of small-bodied ancestors and quickly achieved much greater masses as they diversified into a variety of niches[4]. Thus, the early Palaeocene was likely an important interval in the eutherian transition to placental-like growth strategies, but the life histories of these mammals remain unknown.

Among early placental clades, the Palaeocene–Eocene Pantodonta are a key group, because they were among the first large mammalian herbivores, becoming the largest mammals ever up to that point in time[22]. The early Palaeocene (~62 ma) *Pantolambda bathmodon* (~42 kg) is represented by multiple skeletons representing most of its ontogeny, including a small juvenile with deciduous dentition and unfused epiphyses (New Mexico Museum of Natural History and Science [NMMNH] P-27844; ~17 kg at death). As one of the largest mammals in its ecosystem[23], its life history might provide insight into the relationship between life history and body size in Palaeocene eutherians.

Life histories of extinct animals can be reconstructed using incremental growth features of mineralized tissues like bones and teeth[24–26]. Bones preserve evidence of stress and annual cycles[27,28], and they accurately reflect growth rate throughout life[29,30], including changes associated with maturity[31]. In teeth, daily incremental lines in the dentine and enamel allow for precise chronologies and faithful recording of life history events such as birth and nutritional

stress like that experienced during weaning[32,33], whereas cementum preserves annual growth cycles[24,34]. Chemical signals of birth and early-life diet are recorded in the developing teeth by the abundances of certain trace elements, like zinc (Zn), which is enriched at birth[35,36], and barium (Ba), which varies according to bioavailability in the diet[26]. When integrated with daily growth increments, trace elements maps can reveal birth and the timing of weaning, a technique applied to primates up to 2.6 million years old[9,10,26], but with unrealised potential in other fossil mammals.

Here we combine palaeohistological and geochemical evidence to reconstruct the life history of *P. bathmodon* on a daily scale and evaluate the physiology of a key group in the rise of mammals following the end-Cretaceous mass extinction. These data provide unprecedented insight into the life history of a fossil mammal, revealing that characteristic placental reproductive strategies were established early in their evolution.

Dental development, birth, and weaning

Incremental growth features are well preserved in the teeth, especially the enamel, and are clearly visible in histological thin sections (Fig. 1b–g; Extended Data Fig. 1). Daily laminations in the dentine and enamel[37] (Fig. 1b, c, e) track the successive growth of the tooth crown (Extended Data Table 1). High-resolution trace element mapping of several teeth (Extended Data Table 1; Figs. S1–7) reveals patterns in Zn and Ba that correspond to these incremental growth patterns and provide evidence of birth and weaning in *P. bathmodon* (Fig. 2), extending the viable window for dietary trace element mapping by roughly 60 million years compared to previous studies[10]. The most complete record of early life comes from a second

84 lower molar of an adult individual (NMMNH P-19541), where both the neonatal event and the
85 weaning transition are preserved (Fig. 2).

86 Birth is recorded in the enamel by a prominent neonatal line (Fig. 1g; 2b), a discontinuity
87 in the enamel prisms reflecting developmental disruptions in response to the physiological stress
88 of birth[38]. The neonatal line is Zn-enriched (Fig. 2b; Extended Data Fig. 2), as observed in
89 modern teeth, where this results from changing levels of Zn in serum over the birth interval and
90 the ingestion of Zn-rich colostrum[35,36]. Importantly, the neonatal line is Zn-enriched in multiple
91 cusps of the tooth, and no other accentuated lines in the enamel of this or other teeth are Zn-
92 enriched (Fig. 2b, see Supplement). This suggests that analysis of Zn may be useful as an
93 independent criterion for distinguishing neonatal lines from other accentuated lines in fossil
94 mammals[36].

95 Concentrations of Ba in the enamel are elevated postnatally, but decrease sharply after a
96 short period (Fig. 2c). This pattern is present in both the protoconid and paraconid of the second
97 lower molar, as well as in the first lower molar of the same individual (Fig. 2d), indicating that it
98 represents a consistent biogenic signal. Temporary postnatal Ba enrichment in *P. bathmodon* is
99 identical to that reported in modern and fossil primates[9,10,26], where it reflects the increased
100 bioavailability of Ba in breastmilk[26]. The decrease in Ba presumably marks the onset of weaning
101 and indicates a minimum suckling period of about 31–56 days in *P. bathmodon*. Further
102 independent evidence for a short suckling period also comes from mesowear and microwear in
103 the dentition of a young juvenile (NMMNH P-27844; Extended Data Fig. 3), where growth
104 increments in the dentine of the deciduous teeth are exceptionally well preserved (Fig. 1c;
105 Extended Data Fig. 1). Like in the enamel, a birth signature appears to be recorded in the dentine
106 by a neonatal line, and in this individual the postnatal dentine is Zn-enriched (Extended Data Fig.

4). Dentine continues to infill the pulp cavity throughout life, providing a record of growth both before and after eruption of the tooth and allowing precise estimation of age at death[24]. Approximately 75 daily growth increments separate the neonatal line and the pulp cavity in each tooth of this juvenile skeleton, indicating an age at death of ~2.5 months for this individual. Despite its young age, the presence of dental meso- and microwear[39] (Extended Data Fig. 3) in this individual shows that solid foods (not only milk) were being ingested, providing an upper constraint of 75 days on the onset of weaning.

Aligning daily growth records in the teeth based on the neonatal lines enables the reconstruction of a dental chronology (Fig. 1l). Crown formation times in the teeth are rapid, ranging from 68 days to 183 days (~2–6 months; Extended Data Table 1). All of the deciduous teeth were complete and began erupting before birth, and the first and second adult molars had begun mineralizing. The adult molar crowns were completed within four months after birth and would have begun erupting in the first year. Based on eruption sequences in other pantodonts[40–42], where the third molar erupts last, it is therefore likely that all of the adult teeth of *P. bathmodon* erupted within the first year (see Supplement).

In the permanent teeth of mammals, age at death can be estimated from annual bands in the cementum that anchors the tooth to the jaw[24,34]. Cementum annulations are clearly present in the acellular cementum of most teeth in our sample (Fig. 1d). Most individuals have between two and four annual pairs (Extended Data Table 1), but three individuals with highly worn dentitions compared to other Palaeocene pantodonts have five, seven and possibly as many as eleven pairs, respectively (Extended Data Figure 5; see Supplement).

Skeletal growth

The bone microstructure of the juvenile skeleton (NMMNH P-27844) exhibits densely vascularized fibrolamellar bone, indicating relatively rapid growth (Fig. 1i–k). No annual growth marks are present, consistent with its dental age of ~2.5 months, but a band of more organized, slowly-growing parallel-fibered bone occurs towards the outer surface of the radius and tibia (Fig. 1i; Extended Data Fig. 6), at an estimated mass of 9 kg (see Supplement). External to this band, the bone shows reduced vascularity and relatively slower growth, based on a higher proportion of parallel-fibered matrix (Fig. 1j,k), although laminations in this tissue are not as well developed as in the lamellar bone of the adult individual. This transition likely corresponds to changes in growth rate associated with weaning, as in living ungulates a similar transition occurs in some individuals over this interval[43] (see Supplement). The position of this transition partway through the cortex provides evidence for weaning in this individual prior to death at 2.5 months of age, supporting the 1–2 month suckling period suggested by dental trace elements and tooth wear.

In a skeletally mature adult (NMMNH P-22012), seven annual growth marks are discernible in the exterior cortical bone, matching the number of cementum annulations in its teeth and demonstrating that it was seven years old when it died. The exterior cortex is formed of highly organized lamellar bone, indicating slow growth (Fig. 1h). The earliest annual growth mark is within the slowly-growing exterior cortex (Extended Data Fig. 7), indicating that growth rate decreased significantly before the end of the first year of life. This likely corresponds to the achievement of sexual maturity[31], suggesting that *P. bathmodon* likely reached sexual maturity and approached maximum body size in its first year.

Life history in *Pantolambda bathmodon*

153 Correcting for the onset of tooth mineralization partway through fetal development (see
154 Supplement), the prenatal growth record in the deciduous teeth indicates a gestation period of
155 roughly 207 days or 29.5 weeks. This is an order of magnitude longer than in marsupials or
156 monotremes, but falls close to extant placentals of similar body size (Fig. 3b). Within placentals,
157 gestation length is dichotomous between species that give birth to single or multiple young in
158 each litter[44] (Fig. 3c). The long gestation period in *P. bathmodon* suggests it was likely (posterior
159 probability = 0.96) to have given birth to singleton offspring (see Supplement).
160 Multiple independent lines of evidence from two individuals indicate the onset of
161 weaning between 1–2 months after birth in *P. bathmodon*. Postnatal enrichment in enamel Ba for
162 1–2 months after birth in an adult individual (Fig. 2c, d) is consistent with the development of
163 abrasive microwear and mesowear on the dentition of the 2.5-month old juvenile (Extended Data
164 Fig. 3) and with the transition recorded in its limb bones (Extended Data Fig. 6), identical to
165 weaning transitions recently described on the basis of fluorescent labelling[43]. Together, these
166 lines of evidence constrain weaning in *P. bathmodon* to between 31 and 75 days after birth, with
167 the weight of evidence supporting cessation of suckling by 2 months after birth. The age (31–75
168 days) and mass (9 kg) at weaning in *P. bathmodon* were shorter and smaller than expected for a
169 placental of its adult body mass, but its gestation period (207 days) was slightly longer (Fig. 3a,
170 b). This indicates greater prenatal than postnatal investment in the young, characteristic of
171 placental mammals[7], but also suggests a distinct life history for these early Palaeocene
172 placentals, consistent with other unusual aspects of their biology[45].
173 Most individuals within our sample died between 2–5 years of age (Fig. 1l), suggesting
174 high mortality rates in young animals. The oldest specimen in our sample (estimated to be ~11
175 years old) lived only half the expected lifespan for a mammal of its body mass (20 years; Fig.

3d). This high mortality rate, in conjunction with its short suckling period and rapid onset of sexual maturity (Fig. 3a, e), suggest a fast pace of life in *P. bathmodon*, despite its relatively large size (42 kg).

Combined with its rapid dental and skeletal development, these life history parameters indicate a highly precocial lifestyle in *P. bathmodon*, comparable to the most precocial extant mammals (e.g., deer, giraffes, sheep), which give birth to young with hair and open eyes[13,14]. After a long gestation—the hallmark of the typical placental reproductive mode—a mother *P. bathmodon* likely gave birth to a single, haired offspring with open eyes and well-developed dentition, which nursed for 1–2 months. At ~62 Ma, this constitutes the earliest example of a placentalian-grade physiology in the fossil record.

Growth in early placentals

The growth pattern and rate of *P. bathmodon* differs from both those of Mesozoic mammaliaforms[19,34] and other Cenozoic mammals[46,47]. The mammaliaform *Morganucodon* grew at a much slower rate and for longer period, evidence of a protracted life history more like that of reptiles than mammals[19,34]. Late Cretaceous multituberculates and some eutherians had faster growth rates than *Morganucodon*, but these were still not as rapid as extant mammals[19]. In contrast, *P. bathmodon* exhibits fast growth rates and a rapid developmental schedule, more similar to living precocial placentals. Nonetheless, *P. bathmodon* lived and died faster than expected for a mammal of its body size, outpacing extant mammals and even other extinct mammals from later in the Cenozoic[46,47]. The closest living analogues for *Pantolambda*, independent of mass (Extended Data Fig. 8a), are small antelope, like the neotragines *Madoqua* (Dik-dik) and *Raphicerus* (Steenbok). However, when adult body mass is considered,

Pantolambda is unique among terrestrial mammals (Extended Data Fig. 8b). This life history strategy would have enabled *P. bathmodon* to proliferate at a rapid rate for an animal of its size, which may have been advantageous in the recovering ecosystems of the Palaeocene. Perhaps, as was the case with locomotion[45] and brain size[48], placental life history strategies became limited to their modern range later, as ecosystems saturated.

In contrast to its distinctly rapid pace of life, the gestation period of *P. bathmodon* is remarkably similar to living placentals of its body mass (Fig. 3b; Extended Data Fig. 8), suggesting a more constrained relationship between size and gestation. Indeed, neonate weight and adult body mass are more tightly correlated than other life history parameters in extant placentals (Extended Data Fig. 9), suggesting that neonate weight drives and/or is constrained by adult body mass. As longer gestation enables the larger neonate sizes required for larger adults (Extended Data Fig. 9c), extended gestation periods like that in *P. bathmodon* may have contributed to the rapid increase in body mass in early Palaeocene placentals. The option of extended gestation may have reduced developmental constraints on body size and allowed placentals to expand into vacant niches after the extinction of the non-avian dinosaurs, reaching larger sizes than any Mesozoic mammal[22], and culminating in the largest animals ever[49].

The excellent preservation of daily incremental structures and dietary trace element signatures in a ~62 million year old fossil unlock a new perspective for studying the life history of extinct mammals. Our results suggest that biogenic trace element signals can be retained much longer than previously realized, providing new tools for inferring birth and early-life diet in ancient fossil mammals. Rather than being a limitation for studying reproduction, the abundantly-preserved isolated teeth of Mesozoic mammals may enable combined palaeohistological and geochemical approaches to directly address the evolution of reproduction

in mammals, including its role in their survival at the end-Cretaceous extinction and their radiation thereafter. Indeed, the highly precocial life history of *P. bathmodon* shows that the physiology of at least some close placental relatives had diverged from other mammals by at least the Palaeocene, early in their evolutionary history[21], and suggests that the capacity to increase body size played a role in their ascent from humble Mesozoic beginnings to the dominant role they play in global ecosystems today.

References:

1. Simpson, G. G. The Beginning of the Age of Mammals. *Biol. Rev.* **12**, 1–46 (1937).
2. Grossnickle, D. M., Smith, S. M. & Wilson, G. P. Untangling the Multiple Ecological Radiations of Early Mammals. *Trends Ecol. Evol.* **34**, 936–949 (2019).
3. Halliday, T. J. D. & Goswami, A. Eutherian morphological disparity across the end-Cretaceous mass extinction. *Biol. J. Linn. Soc.* **118**, 152–168 (2016).
4. Alroy, J. The fossil record of North American mammals: evidence for a Paleocene evolutionary radiation. *Syst. Biol.* **48**, 107–118 (1999).
5. Slater, G. J. Phylogenetic evidence for a shift in the mode of mammalian body size evolution at the Cretaceous-Palaeogene boundary. *Methods Ecol. Evol.* **4**, 734–744 (2013).
6. Williamson, T. E., Brusatte, S. L., Carr, T. D., Weil, A. & Standhardt, B. R. The phylogeny and evolution of Cretaceous–Palaeogene metatherians: cladistic analysis and description of new early Palaeocene specimens from the Nacimiento Formation, New Mexico. *J. Syst. Palaeontol.* **10**, 625–651 (2012).
7. Langer, P. The phases of maternal investment in eutherian mammals. *Zoology* **111**, 148–162 (2008).

8. Lillegraven, J. A., Thompson, S. D., McNAB, B. K. & Patton, J. L. The origin of eutherian mammals. *Biol. J. Linn. Soc.* **32**, 281–336 (1987).
9. Austin, C. *et al.* Barium distributions in teeth reveal early-life dietary transitions in primates. *Nature* **498**, 216–219 (2013).
10. Joannes-Boyau, R. *et al.* Elemental signatures of *Australopithecus africanus* teeth reveal seasonal dietary stress. *Nature* **572**, 112–115 (2019).
11. Burgin, C. J., Colella, J. P., Kahn, P. L. & Upham, N. S. How many species of mammals are there? *J. Mammal.* **99**, 1–14 (2018).
12. Lillegraven, J. A. Biological considerations of the marsupial-placental dichotomy. *Evolution* **29**, 707–722 (1975).
13. Werneburg, I., Laurin, M., Koyabu, D. & Sánchez-Villagra, M. R. Evolution of organogenesis and the origin of altriciality in mammals: mammalian embryology. *Evol. Dev.* **18**, 229–244 (2016).
14. Ferner, K., Schultz, J. A. & Zeller, U. Comparative anatomy of neonates of the three major mammalian groups (monotremes, marsupials, placentals) and implications for the ancestral mammalian neonate morphotype. *J. Anat.* **231**, 798–822 (2017).
15. Cooper, W. J. & Steppan, S. J. Developmental constraint on the evolution of marsupial forelimb morphology. *Aust. J. Zool.* **58**, 1 (2010).
16. Fabre, A.-C. *et al.* Functional constraints during development limit jaw shape evolution in marsupials. *Proc. R. Soc. B Biol. Sci.* **288**, rspb.2021.0319, 20210319 (2021).
17. Simmons, N. B., Seymour, K. L., Habersetzer, J. & Gunnell, G. F. Primitive early Eocene bat from Wyoming and the evolution of flight and echolocation. *Nature* **451**, 818–821 (2008).

18. Thewissen, J. G. M., Williams, E. M., Roe, L. J. & Hussain, S. T. Skeletons of terrestrial cetaceans and the relationship of whales to artiodactyls. *Nature* **413**, 277–281 (2001).
19. Chinsamy, A. & Hurum, J. H. Bone microstructure and growth patterns of early mammals. *Acta Palaeontol. Pol.* **51**, 325–338 (2006).
20. Novacek, M. J. *et al.* Epipubic bones in eutherian mammals from the Late Cretaceous of Mongolia. *Nature* **389**, 483–486 (1997).
21. O'Leary, M. A. *et al.* The placental mammal ancestor and the post–K-Pg radiation of placentals. *Science* **339**, 662–667 (2013).
22. Smith, F. A. *et al.* The evolution of maximum body size of terrestrial mammals. *Science* **330**, 1216–1219 (2010).
23. Shelley, S. L., Williamson, T. E. & Brusatte, S. L. The osteology of *Periptychus carinidens*: a robust, ungulate-like placental mammal (Mammalia: Periptychidae) from the Paleocene of North America. *PLOS ONE* **13**, e0200132 (2018).
24. Klevezal, G. A. *Recording structures of mammals: determination of age and reconstruction of life history*. (Balkema, 1996).
25. Padian, K. & Lamm, E.-T. *Bone histology of fossil tetrapods: advancing methods, analysis, and interpretation*. (University of California Press, 2013).
26. Smith, T. M., Cook, L., Dirks, W., Green, D. R. & Austin, C. Teeth reveal juvenile diet, health and neurotoxicant exposure retrospectively: what biological rhythms and chemical records tell us. *BioEssays* 2000298 (2021) doi:10.1002/bies.202000298.
27. Nacarino-Meneses, C. & Köhler, M. Limb bone histology records birth in mammals. *PLoS ONE* **13**, e0198511 (2018).

28. Köhler, M., Marín-Moratalla, N., Jordana, X. & Aanes, R. Seasonal bone growth and physiology in endotherms shed light on dinosaur physiology. *Nature* **487**, 358–361 (2012).
29. de Margerie, E. Assessing a relationship between bone microstructure and growth rate: a fluorescent labelling study in the King Penguin chick (*Aptenodytes patagonicus*). *J. Exp. Biol.* **207**, 869–879 (2004).
30. Castanet, J., Cubo, J. & Montes, L. Relationship between bone growth rate and bone tissue organization in amniotes: first test of Amprino's rule in a phylogenetic context. *Anim. Biol.* **60**, 25–41 (2010).
31. Calderón, T., DeMiguel, D., Arnold, W., Stalder, G. & Köhler, M. Calibration of life history traits with epiphyseal closure, dental eruption and bone histology in captive and wild red deer. *J. Anat.* **235**, 205–216 (2019).
32. Dirks, W., Humphrey, L. T., Dean, M. C. & Jeffries, T. E. The relationship of accentuated lines in enamel to weaning stress in juvenile baboons (*Papio hamadryas anubis*). *Folia Primatol. (Basel)* **81**, 207–223 (2010).
33. Schwartz, G. T., Reid, D. J., Dean, M. C. & Zihlman, A. L. A faithful record of stressful life events preserved in the dental development record of a juvenile gorilla. *Int. J. Primatol.* **27**, 1221–1222 (2006).
34. Newham, E. *et al.* Reptile-like physiology in Early Jurassic stem-mammals. *Nat. Commun.* **11**, 5121 (2020).
35. Dean, M. C., Spiers, K. M., Garrevoet, J. & Le Cabec, A. Synchrotron X-ray fluorescence mapping of Ca, Sr and Zn at the neonatal line in human deciduous teeth reflects changing perinatal physiology. *Arch. Oral Biol.* **104**, 90–102 (2019).

36. Smith, T. M. *et al.* Permanent signatures of birth and nursing initiation are chemically recorded in teeth. *J. Archaeol. Sci.* **140**, 105564 (2022).
37. Tafforeau, P., Bentaleb, I., Jaeger, J.-J. & Martin, C. Nature of laminations and mineralization in rhinoceros enamel using histology and X-ray synchrotron microtomography: potential implications for palaeoenvironmental isotopic studies. *Palaeogeogr. Palaeoclimatol. Palaeoecol.* **246**, 206–227 (2007).
38. Schour, I. The neonatal line in the enamel and dentin of the human deciduous teeth and first permanent molar. *J. Am. Dent. Assoc. 1922* **23**, 1946–1955 (1936).
39. Scott, R. M. & Halcrow, S. E. Investigating weaning using dental microwear analysis: a review. *J. Archaeol. Sci. Rep.* **11**, 1–11 (2017).
40. Mao, F., Wang, Y.-Q., Meng, J. & Jin, X. Tooth crown formation time in three Asian coryphodontids, and its implication for identifying living analogues. *Vertebr. Palasiat.* **42**, 153–170 (2014).
41. Lucas, S. G. & Schoch, R. M. Ontogenetic studies of early Cenozoic *Coryphodon* (Mammalia, Pantodonta). *J. Paleontol.* **64**, 831–841 (1990).
42. Muizon, C. D. & Marshall, L. G. *Alcidedorbignya inopinata* (Mammalia: Pantodonta) from the Early Paleocene of Bolivia: phylogenetic and paleobiogeographic implications. *J. Paleontol.* **66**, 499–520 (1992).
43. Calderón, T., Arnold, W., Stalder, G., Painer, J. & Köhler, M. Labelling experiments in red deer provide a general model for early bone growth dynamics in ruminants. *Sci. Rep.* **11**, 14074 (2021).
44. Müller, D. W. H. *et al.* Dichotomy of eutherian reproduction and metabolism. *Oikos* **121**, 102–115 (2012).

45. Shelley, S. L., Brusatte, S. L. & Williamson, T. E. Quantitative assessment of tarsal morphology illuminates locomotor behaviour in Palaeocene mammals following the end-Cretaceous mass extinction. *Proc. R. Soc. B Biol. Sci.* **288**, rspb.2021.0393, 20210393 (2021).
46. Kolb, C. *et al.* Mammalian bone palaeohistology: a survey and new data with emphasis on island forms. *PeerJ* **3**, e1358 (2015).
47. Dirks, W., Anemone, R. L., Holroyd, P. A., Reid, D. J. & Walton, P. Phylogeny, life history and the timing of molar crown formation in two archaic ungulates, *Meniscotherium* and *Phenacodus* (Mammalia, 'Condylarthra'). in *Comparative Dental Morphology* (eds. Meyer, G., Koppe, T. & Alt, K. W.) vol. 13 3–8 (KARGER, 2009).
48. Bertrand, O. C. *et al.* Brawn before brains in placental mammals after the end-Cretaceous extinction. *Science* **376**, 80–85 (2022).
49. Smith, F. A. & Lyons, S. K. How big should a mammal be? A macroecological look at mammalian body size over space and time. *Philos. Trans. R. Soc. B Biol. Sci.* **366**, 2364–2378 (2011).

Figure Captions:

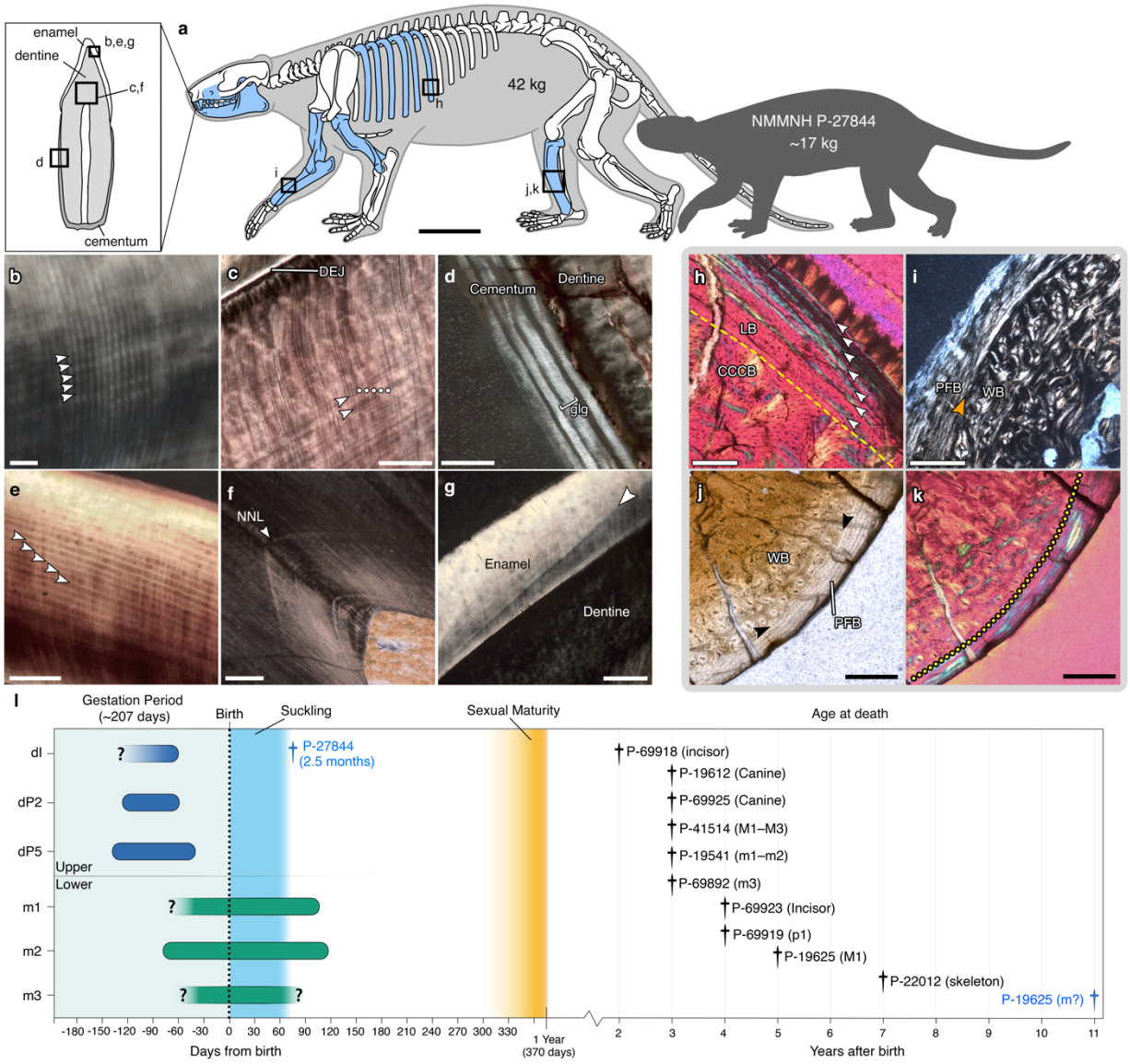

Fig. 1. Palaeohistology of *Pantolambda bathmodon*. (a) Skeletal reconstruction of adult with sampled elements in blue; boxes show representative locations of palaeohistological images, silhouette shows relative size of juvenile NMMNH P-27844. (b–g) dental features used for reconstruction of life history (all coronal sections): (b) enamel cross-striations (arrows) in second lower molar of NMMNH P-19541; (c) lines of von Ebner in deciduous ultimate upper premolar of NMMNH P-27844, white dots mark five lines and arrows show orientation of lines; (d)

cementum annulations (one light + one dark band) in first lower premolar of NMMNH P-69919; (e) daily laminations (arrows) in lower incisor of NMMNH P-69918; (f) neonatal line in dentine of deciduous ultimate upper premolar of NMMNH P-27844; and (g) neonatal line (arrow) in enamel of second lower molar of NMMNH P-19541. (h–k), osteohistological features used for reconstruction of life history (all transverse midshaft diaphysis sections): (h) lines of arrested growth (arrows) in outer cortex of rib of NMMNH P-22012; (i) annulus (orange arrow) at weaning transition in radius of NMMNH P-27844; (j–k) weaning transition (arrows and yellow line) in outer cortex of tibia of NMMNH P-27844 under plane polarized light (j) and cross-polarized light with a lambda filter (k). Images (b–g, i) under cross-polarized light, (h) under cross-polarized light with a lambda filter. (l) life history chronology of *P. bathmodon* showing crown formation times for deciduous (blue) and adult (green) teeth, life history events, and mortality. Daggers indicate ages at death, youngest and oldest specimens highlighted in blue. **Abbreviations: CCCB,** compact coarse cancellous bone; **DEJ**, dentinoenamel junction; **WB**, woven-fibered bone; **glg**, growth layer group; **LB**, lamellar bone; **NNL**, neonatal line; **PFB**, parallel-fibered bone. Scale bars: 10 cm (a), 25 μm (b), 50 μm (e), 100 μm (c, d), 200 μm (f–h), 500 μm (i–k).

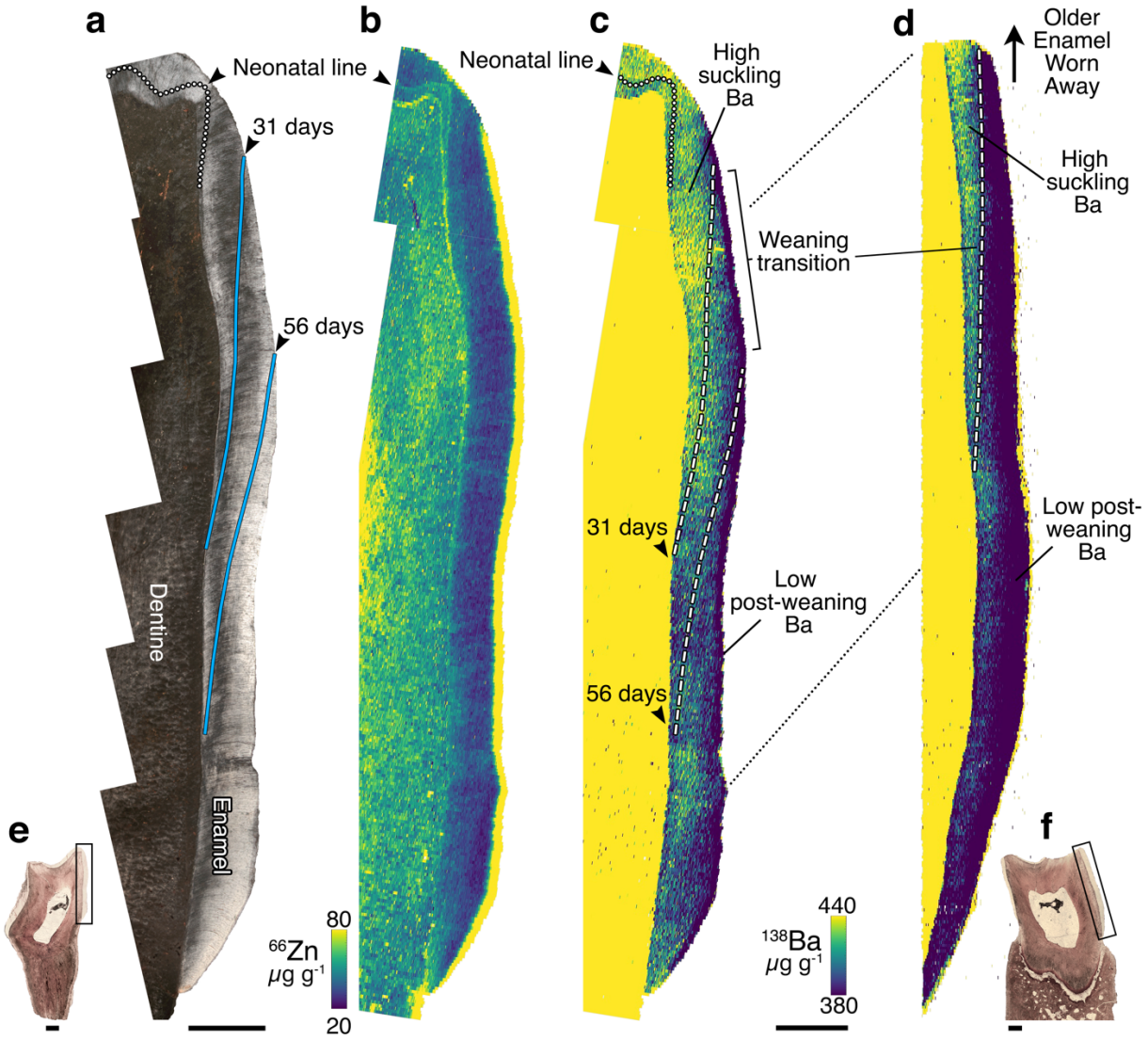

Fig. 2. Trace element distributions in the enamel of the first and second lower molars (NMMNH P-19541; also see Figs. S1–3). (a) Thin section under cross-polarized light shows clear daily laminations and the neonatal line (dotted line) in the enamel of the paraconid of the second lower molar. (b) Trace element map of Zn shows enrichment at the neonatal line. (c) Barium is enriched in early postnatal enamel (also see Supplementary Fig. S8), but decreases gradually between 31–56 days after birth (dashed lines). (d) The transition between high and low Ba is clearer in the paraconid of the first lower molar of the same individual, where older enamel

including the neonatal line has been worn away. (e,f) overview images showing position of images within first (f) and second (e) lower molars. Scale bars: 500 µm (a–d), 1 mm (e, f).

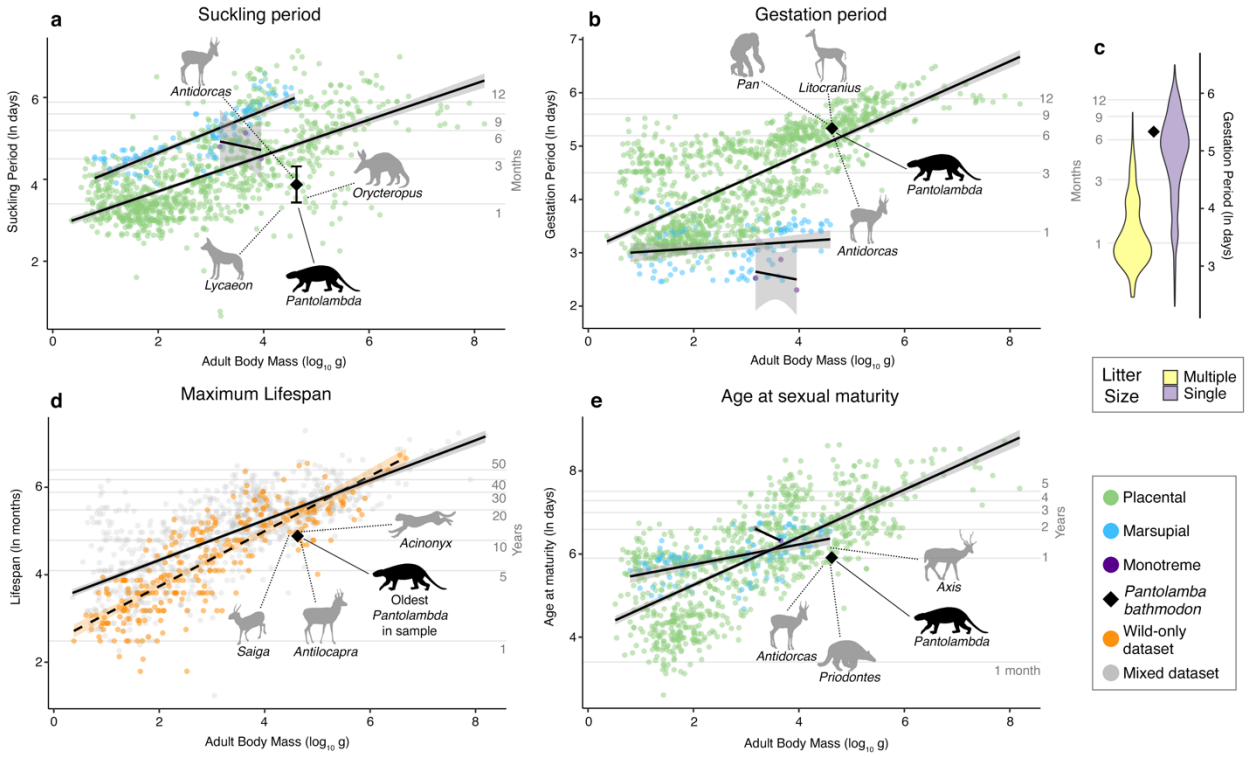

Fig. 3. Comparison of the reconstructed life history of *Pantolambda bathmodon* (black diamonds) to extant mammals using the PanTheria Dataset[50]. Suckling period, showing the range (31–75 days) estimated for *P. bathmodon* based on dental trace elements, bone histology, and dental wear (a); gestation period (b), violin plot of gestation period sorted by litter size (c), maximum lifespan, showing data from PanTHERIA (grey, solid line) and from the wild-only lifespan dataset of Newham et al.[34] (orange, dashed regression line) (d), and age at sexual maturity (e) for living mammals (green: placentals; blue: marsupials; purple: monotremes) plotted against adult body mass (log_{10} g). Trendlines show generalized linear model regressions for placentals, marsupials, and monotremes, with 95% confidence intervals for the regression indicated by shaded envelopes. Horizontal lines show untransformed values. Silhouettes for each

399 panel show living taxa similar in the reconstructed parameter to the estimate for *P. bathmodon*.
400 Silhouette of *Pantolambda bathmodon* created by SLS. Silhouettes of *Acinonyx*, *Antilocapra*,
401 *Lycaeon*, *Orycteropus*, *Pan*, *Priodontes* have been adapted from Phylopic images (CC0 1.0
402 https://creativecommons.org/publicdomain/zero/1.0/), silhouette of *Litocranius* is original
403 artwork by GFF, and all others were generated from public domain images (CC0 1.0
404 https://creativecommons.org/publicdomain/zero/1.0/).
405
406
407 **Methods:**
408 We prepared thin sections (see Supplementary Information) of the teeth and bones of 12
409 specimens of *Pantolambda bathmodon*, including two partial skeletons and totalling 45 elements
410 (23 bones and 22 teeth), collected from the Torrejonian NALMA of the Nacimiento Formation in
411 the San Juan Basin of New Mexico, USA[51]. The specimens were selected to represent as much of
412 the skeleton and as many tooth positions as possible and to capture varying degrees of dental
413 wear, presumably attributable to individuals of different ages. The minimum number of
414 individuals based on skeletal overlap *a priori* was three, but age variation indicates a minimum
415 of seven individuals in our palaeohistological sample.
416 Incremental marks in the cementum, dentine, and enamel were counted from thin-
417 sections to assess the timing and pace of tooth development. Cementum annulations, lines of von
418 Ebner in the dentine, and cross-striations in the enamel were each clearly visible under cross-
419 polarized light. Pairs of one light and one dark band in the acellular extrinsic fiber cementum
420 near the cervix of the tooth were counted as growth layer groups representing annual growth
421 cycles[24,52,53]. Lines of von Ebner in the dentine, clearly distinct from more broadly spaced

Andresen lines[24,54], were counted from high-magnification photomontages as daily increments of growth. Likewise, cross-striations in the enamel were interpreted as daily increments of growth[54,55]. In every specimen, enamel cross-striations were aligned into clearly visible growth laminations, which have a daily periodicity[37,56]. The neonatal line in the enamel was identified as a prominent, Zn-enriched[35] accentuated line formed by discontinuities in the enamel prisms. In the dentine of the deciduous teeth, the earliest accentuated stress line was identified as the neonatal line[24], which was supported by consistent changes in Zn concentration across the neonatal boundary[35,57] (Extended Data Fig. 4). The neonatal line was used to demarcate pre- and post-natal developmental periods, and to align sequences from different tooth positions within and between individuals. Daily growth increments in the enamel were traced from high-resolution photomontages to create temporal maps of daily dental development for each tooth. Enamel secretion, crown extension, and crown formation rates were estimated using the methods of Dirks et al.[47]

Dietary trace element concentrations were assessed using laser-ablation inductively coupled-plasma mass spectroscopy (LA-ICP-MS) at the University of Edinburgh and the University of St. Andrews Isotope Geochemistry (STAiG) lab. After pilot runs using an ATLEX-I-LR Analyte Excite 193 nm ArF excimer coupled to an Attom ICPMS, Nu Instrument at the University of Edinburgh, to assess the suitability of the material for analysis, a broad array of trace element concentrations (^{11}B, ^{23}Na, ^{25}Mg, ^{27}Al, ^{31}P, ^{43}Ca, ^{46}Ca, ^{55}Mn, ^{59}Co, ^{60}Ni, ^{63}Cu, ^{66}Zn, ^{88}Sr, ^{89}Y, ^{138}Ba, ^{208}Pb, and ^{238}U) in the enamel and dentine of six teeth were mapped using LA-ICP-MS on an Agilent 8900-QQQ at the STAiG lab. Entire enamel sequences of three teeth (the paraconid of a lower first molar [NMMNH P-19541], the protoconid of a lower second molar [NMMNH P-19541], and the labial enamel of an incisor [NMMNH P-69918]) were scanned at

high resolution (20 μm spot size, 10 μm s^{-1} scanning speed, ICP cycle time 0.2889 s), with an effective pixel size of 60 μm^2 (Figs. S1–4). Small regions of interest in the deciduous teeth (NMMNH P-27844) were also scanned at high resolution (38 μm spot size, 38 μm s^{-1} scanning speed; Figs. S5–7). LA-ICP-MS data were processed and rasterized in Iolite v4.5.5.4[58]. Concentrations were normalized to and drift-corrected by a NIST 612 glass standard after gas blank subtraction, and standardized to ~40% Ca. Elemental maps and transects were registered to temporal maps of dental development to evaluate daily changes in diet.

Dental microwear was evaluated using scanning electron microscopy (SEM) using a Carl Zeiss SIGMA DH VP field emission SEM at the University of Edinburgh operated at 15 kV for secondary electron imaging of the fine-scale features of the occlusal surface of the first upper molar of NMMNH P-27844.

Reconstructed life history parameters for *P. bathmodon* were plotted alongside data from the PanTHERIA dataset[50] for comparison. Because the PanTHERIA dataset includes mostly captive individuals, which are likely to have greater maximum lifespans than wild individuals, the estimated maximum lifespan of *P. bathmodon* was also compared to a recent wild-only dataset of mammal maximum lifespan[34]. Relative importance of life history parameters for predicting body size was evaluated using multiple regression, and litter size was predicted using linear discriminant analysis based on gestation period. Principal components analysis was used to identify the closest living analogues of *P. bathmodon*.

50. Jones, K. E. *et al.* PanTHERIA: a species-level database of life history, ecology, and geography of extant and recently extinct mammals. *Ecology* **90**, 2648–2648 (2009).

51. Williamson, T. E. *The beginning of the age of mammals in the San Juan Basin, New Mexico: biostratigraphy and evolution of Paleocene mammals of the Nacimiento Formation*. vol. 8 (New Mexico Museum of Natural History and Science, 1996).
52. Newham, E. *et al.* Synchrotron radiation-based X-ray tomography reveals life history in primate cementum incrementation. *J. R. Soc. Interface* **17**, 20200538 (2020).
53. Berkovitz, B. & Shellis, P. Teeth and life history. in *The Teeth of Mammalian Vertebrates* 305–321 (Elsevier, 2018). doi:10.1016/B978-0-12-802818-6.00016-8.
54. Dean, M. C. Tooth microstructure tracks the pace of human life-history evolution. *Proc. R. Soc. B Biol. Sci.* **273**, 2799–2808 (2006).
55. Smith, T. M. Teeth and human life-history evolution. *Annu. Rev. Anthropol.* **42**, 191–208 (2013).
56. Emken, S., Witzel, C., Kierdorf, U., Frölich, K. & Kierdorf, H. Characterization of short-period and long-period incremental markings in porcine enamel and dentine—Results of a fluorochrome labelling study in wild boar and domestic pigs. *J. Anat.* **239**, 1207–1220 (2021).
57. Lochner, F., Appleton, J., Keenan, F. & Cooke, M. Multi-element profiling of human deciduous teeth by laser ablation-inductively coupled plasma-mass spectrometry. *Anal. Chim. Acta* **401**, 299–306 (1999).
58. Paton, C., Hellstrom, J., Paul, B., Woodhead, J. & Hergt, J. Iolite: Freeware for the visualisation and processing of mass spectrometric data. *J. Anal. At. Spectrom.* **26**, 2508 (2011).

Acknowledgments We thank N. Volden for facilitating specimen access, J. Craven for access to microscopy facilities, and A. Reynolds for discussion of captive lifespan. Funding was provided by the University of Edinburgh, the Royal Society [Grant NIF\R1\191527], National Science Foundation [Grants DEB 1654949 and EAR 1654952], European Research Council (ERC) Starting Grants [No. 756226 and 805246] under the European Union's Horizon 2020 Research and Innovation Programme, a Philip Leverhulme Prize and a SNSF Mobility Fellowship [Grant P2EZP2_199923].

Author contributions G.F.F. designed the study, made the thin sections, conducted the histological, life history, and statistical analyses, prepared the figures, and wrote the manuscript; P.E.dP. contributed to the study design, identification of the material, morphological analyses, and the drafting of the manuscript; J.T.S. and M.D. conducted the LA-ICP-MS analyses at STAiG and contributed to figures and drafting the manuscript; S.L.S. created the skeletal reconstruction of *P. bathmodon* and contributed to discussion and drafting the manuscript; L.E.P. conducted the LA-ICP-MS analyses at the University of Edinburgh and contributed to drafting the manuscript; N.J.C. conducted the SEM analyses; J.R.W. contributed to drafting the manuscript; T.E.W. oversaw the collection and curation of the material, provided stratigraphic data and contributed to drafting the manuscript; J.W.B.R. supervised the LA-ICP-MS analyses; S.L.B. coordinated the project and contributed to study design and drafting the manuscript.

Competing interests The authors declare no competing interests.

Data availability Fossil specimens in this study are housed at the New Mexico Museum of Natural History and Science, and the palaeohistological thin sections underlying the analyses are accessioned at the University of Edinburgh but will be returned to the NMMNH for permanent curation upon completion of our research. The living mammal datasets are available from Jones et al.[50] (https://doi.org/10.6084/m9.figshare.c.3301274.v1) and Newham et al.[34] (https://www.nature.com/articles/s41467-020-18898-4#Sec18). Overview images of palaeohistological slides and LA-ICP-MS data are deposited at Figshare (doi: 10.6084/m9.figshare.20272737).

Code availability No custom code or software was used in the study.

Additional information

Supplementary information Supplementary Information is available for this paper.

Correspondence and requests for materials should be addressed to G.F.F. (Gregory.Funston@ed.ac.uk; funston@ualberta.ca; funston.paleo@gmail.com) or S.L.B (Stephen.Brusatte@ed.ac.uk).

Peer review information

Extended Data Captions:

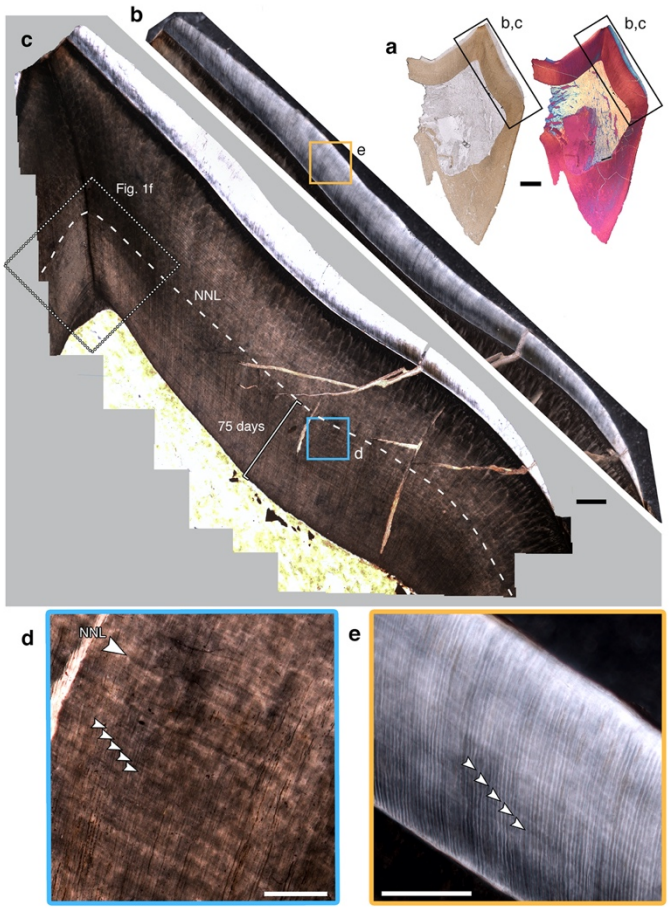

Extended Data Fig. 1. Incremental features of the teeth of *Pantolambda bathmodon*. (a) Overview of coronal section of deciduous ultimate upper premolar of NMMNH P-27844 under plane-polarized light (left) and cross-polarized light with a lambda filter (right), showing locations of inset images. (b,c) Photomontages of the protocone exposed for the enamel (b) and the dentine (c), showing excellent preservation of incremental features, neonatal line (dashed line), and locations of close-up images. (d) Contrast-enhanced close-up of lines of von Ebner preserved in the dentine (arrows), extending parallel to the dentinoenamel junction and perpendicular to dentine tubules, and neonatal line (large arrow). (e) Contrast-enhanced close-up of enamel cross-striations and daily laminations (arrows) in the enamel, extending sub-parallel to

the dentinoenamel junction and perpendicular to the enamel prisms. **Abbreviations: NNL**, neonatal line. Scale bars: 1 mm (a), 200 µm (b, c), 100 µm (d, e).

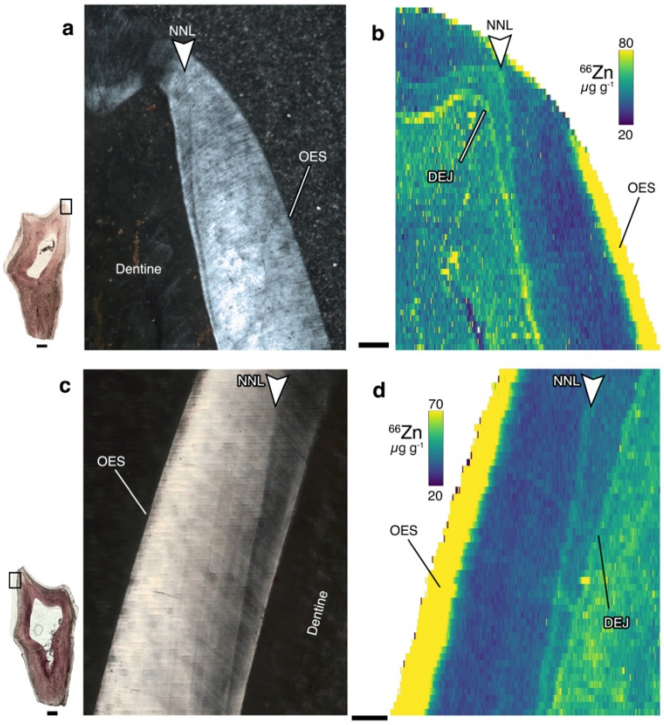

Extended Data Fig. 2. Zn-enrichment of the neonatal line in the enamel of lower second molar of NMMNH P-19541. (a, c) coronal sections of enamel of paraconid (a) and protoconid (c) under cross-polarized light. Insets show location on coronal sections of entire tooth. (b, d), LA-ICP-MS trace element maps, showing higher concentrations of Zn in discrete areas corresponding to the neonatal line (white arrows). **Abbreviations: DEJ,** dentinoenamel junction; **NNL**, neonatal line; **OES**, outer enamel surface. Scale bars: 1 mm (insets), 100 µm (a–d).

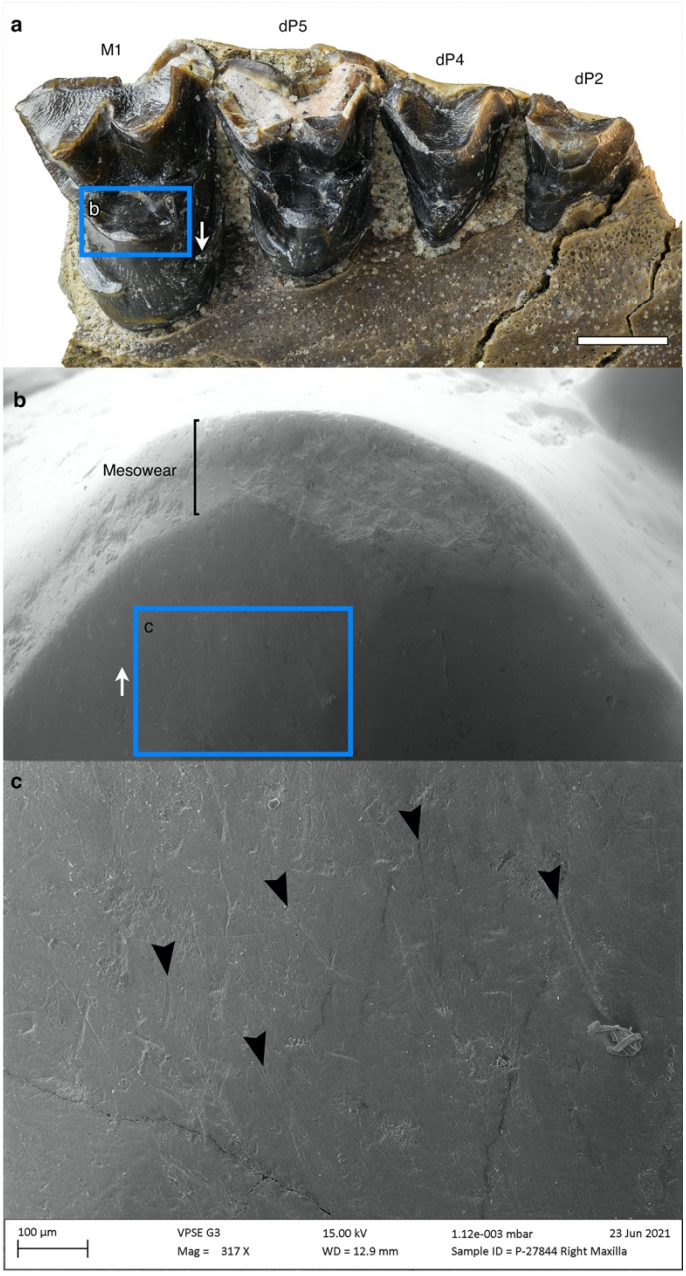

551

552 **Extended Data Fig. 3.** Microwear on the dentition of NMMNH P-27844. (a) Right maxilla with
553 three deciduous premolars and adult first molar in occlusal view, showing location of scanning
554 electron microscopy (SEM) scan. (b) Overview secondary electron (SE) image of protocone of
555 adult first molar, showing development of mesowear and location of close-up image. (c) Close-
556 up SE image of scratches and gouges attributable to abrasive microwear; black arrows highlight

curved scratches resulting from chewing motion. White arrows in (a) and (b) indicate lingual direction. **Abbreviations: d**, deciduous; **M**, upper molar; **P**, upper premolar.

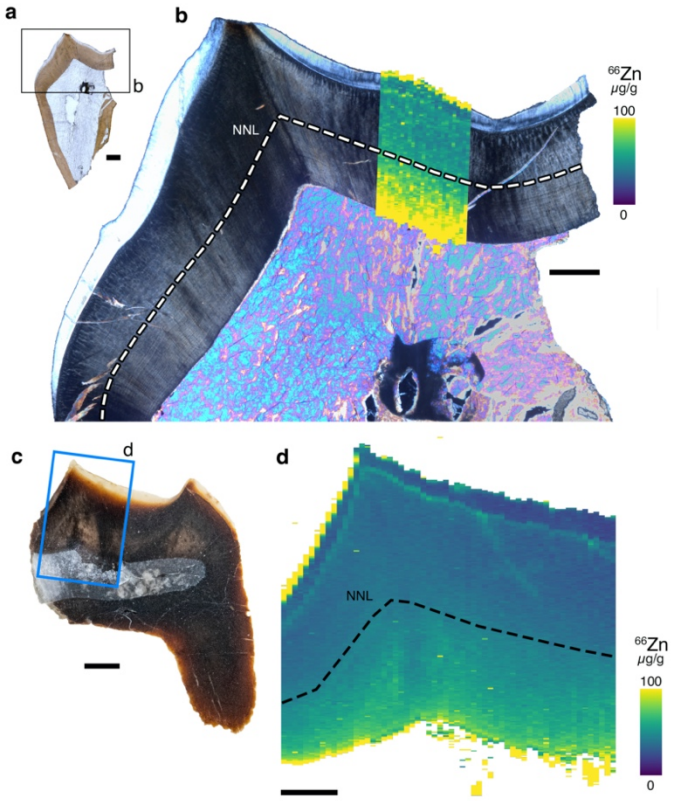

Extended Data Fig. 4. Changes in zinc associated with birth in the deciduous upper premolars of NMMNH P-27844. Postnatal dentine is enriched in Zn in the deciduous upper ultimate premolar (a, b) and the deciduous upper second premolar (c, d). (a) Overview of thin section showing location of close-up image. (b) Mosaic image showing protocone in cross-polarized light, with trace element map overlain, showing change at histologically-inferred neonatal line (dashed line; NNL). (c) Overview image of embedded block showing location of trace element map. (d) Trace element map showing increased postnatal Zn. Scale bars: 1 mm (a, c), 500 μm (b, d). **Abbreviations: NNL**, neonatal line.

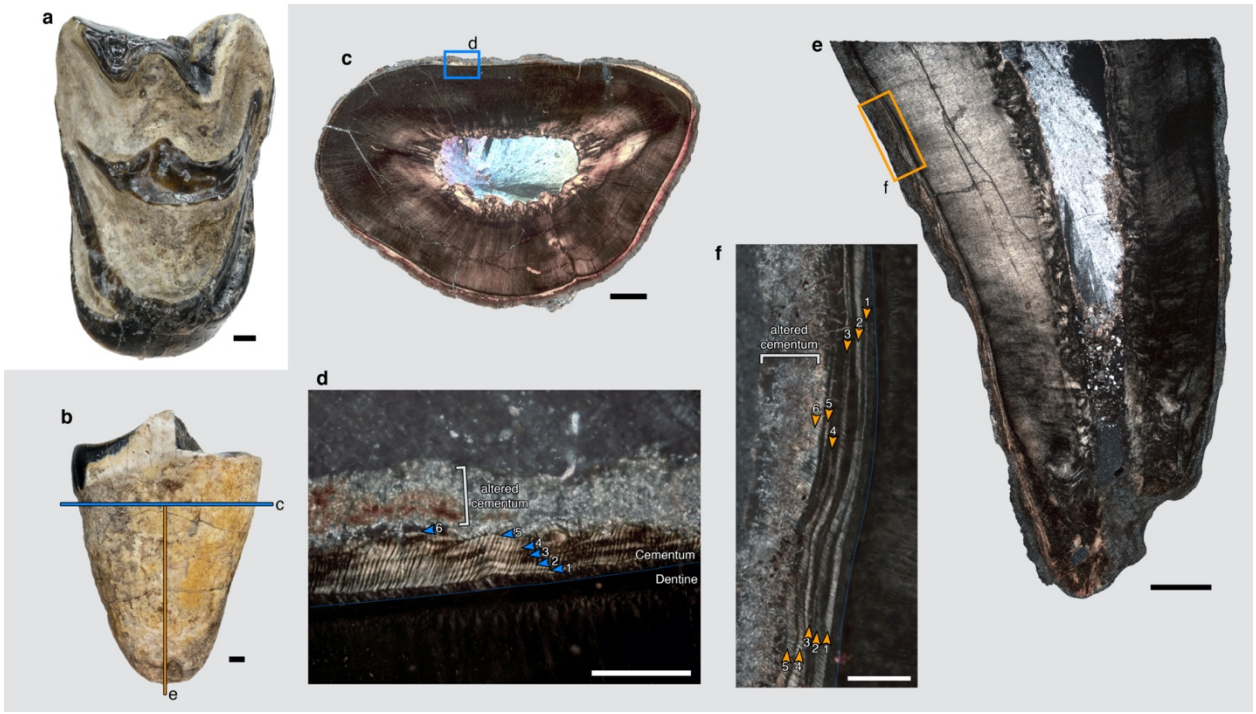

Extended Data Fig. 5. Dental wear, cementum annulations, and maximum lifespan in the oldest sampled individuals. (a) Right first upper molar of NMMNH P-19625, showing extensive wear and erosion of enamel in most areas of the crown. (b) Anterior root of lower molar (tooth position unknown) from another individual of NMMNH P-19625, showing the location of the thin sections. (c) Overview transverse section of cervical root area, showing clear demarcation of cementum and dentine, and location of close-up. (d) Close-up of acellular extrinsic-fiber cementum in transverse section, showing six pairs of dark and bright bands comprising annual growth layer groups and alteration of external cementum; bright bands indicated with blue arrows. (e) longitudinal section of the same tooth, showing thick external layer of cementum, continuity of growth layer groups, and location of close-up. (f) close-up image of acellular extrinsic-fiber cementum in longitudinal section, showings six annual growth layer groups and alteration of external cementum; birght bands indicated with orange arrows. Images c–f under cross-polarized light. Scale bars: 1 mm (a–c, e), 200 µm (d, f).

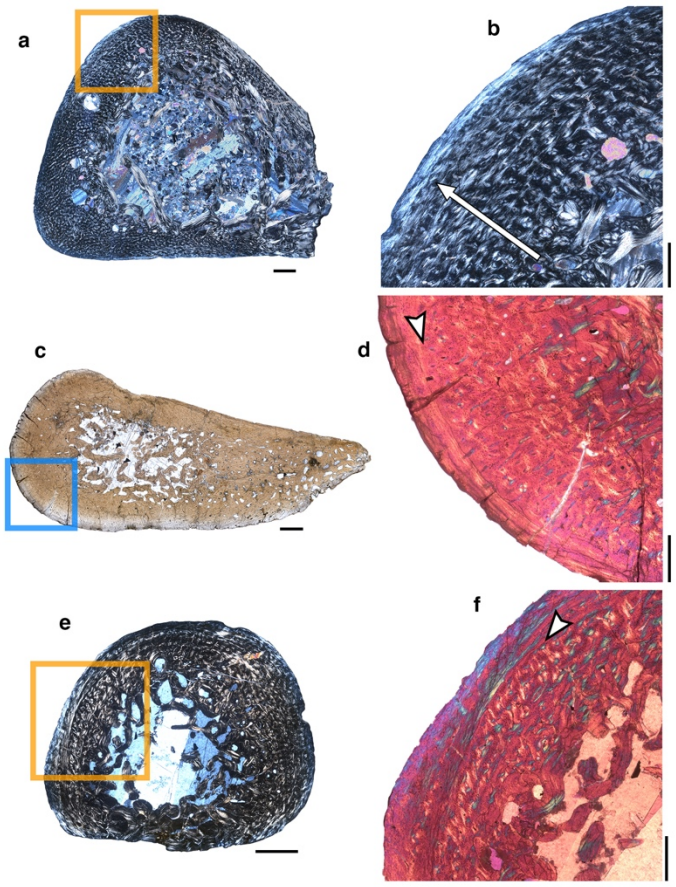

Extended Data Fig. 6. Weaning transition recorded in the postcranial bones of NMMNH P-27844. (a) Transverse section of right humerus diaphysis under cross-polarized light, showing arrangement of tissues and large medullary cavity and location of close-up image. (b) Close-up of cortex of right humerus under cross-polarized light, showing increase in proportion of parallel-fibered bone (brighter tissues) later in growth (arrow), indicative of a decrease in growth rate. (c) Transverse section of right tibia diaphysis under plane polarized light, showing location of close-up image. (d) Close-up of cortex of right tibia under cross-polarized light with a lambda filter, showing transition (arrow) from highly-vascularized fibrolamellar bone with a high proportion of woven-fibered matrix (upper right) to more slowly-growing parallel-fibered bone with reduced vascularity (lower left). (e) Transverse section of right radius diaphysis under cross-polarized light, showing location of close-up image. (f) Close-up image of cortex of right

radius under cross-polarized light with a lambda filter, showing annulus of parallel-fibered bone (arrow) separating region of highly-vascularized fibrolamellar bone (lower right) from region of less-vascularized fibrolamellar bone with a higher proportion of parallel-fibered bone (upper left). Scale bars: 1 mm (a, c, e), 500 µm (b, d, f).

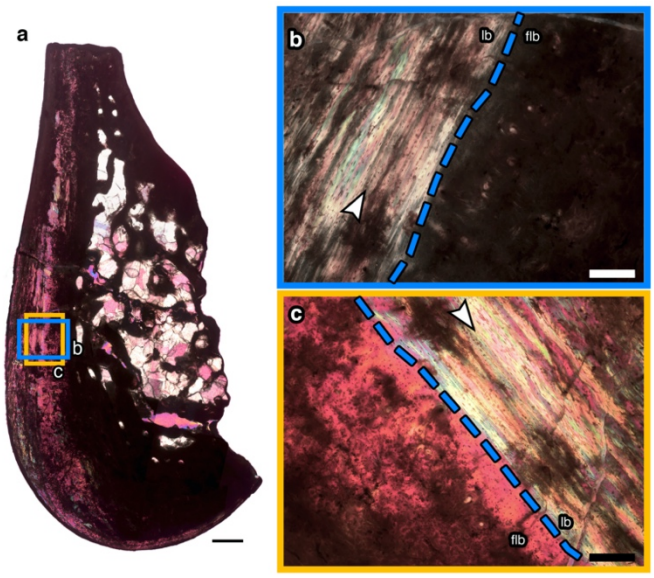

Extended Data Fig. 7. Transition to slower growth likely reflecting sexual maturity. (a) Coronal section of posterior dentary of NMMNH P-22012 under cross-polarized light with a lambda filter, showing locations of close-up images. Dark regions have been diagenetically altered by the deposition of opaque minerals. (b, c) Close-up of transition (dashed line) between faster-growing fibrolamellar bone (flb) and slower-growing lamellar bone (lb), indicative of sexual maturity, under cross-polarized light (b) and cross-polarized light with a lambda filter (c). Arrows indicate first line of arrested growth, deposited after the transition to slower growth. Scale bars: 1 mm (a), 200 µm (b, c).

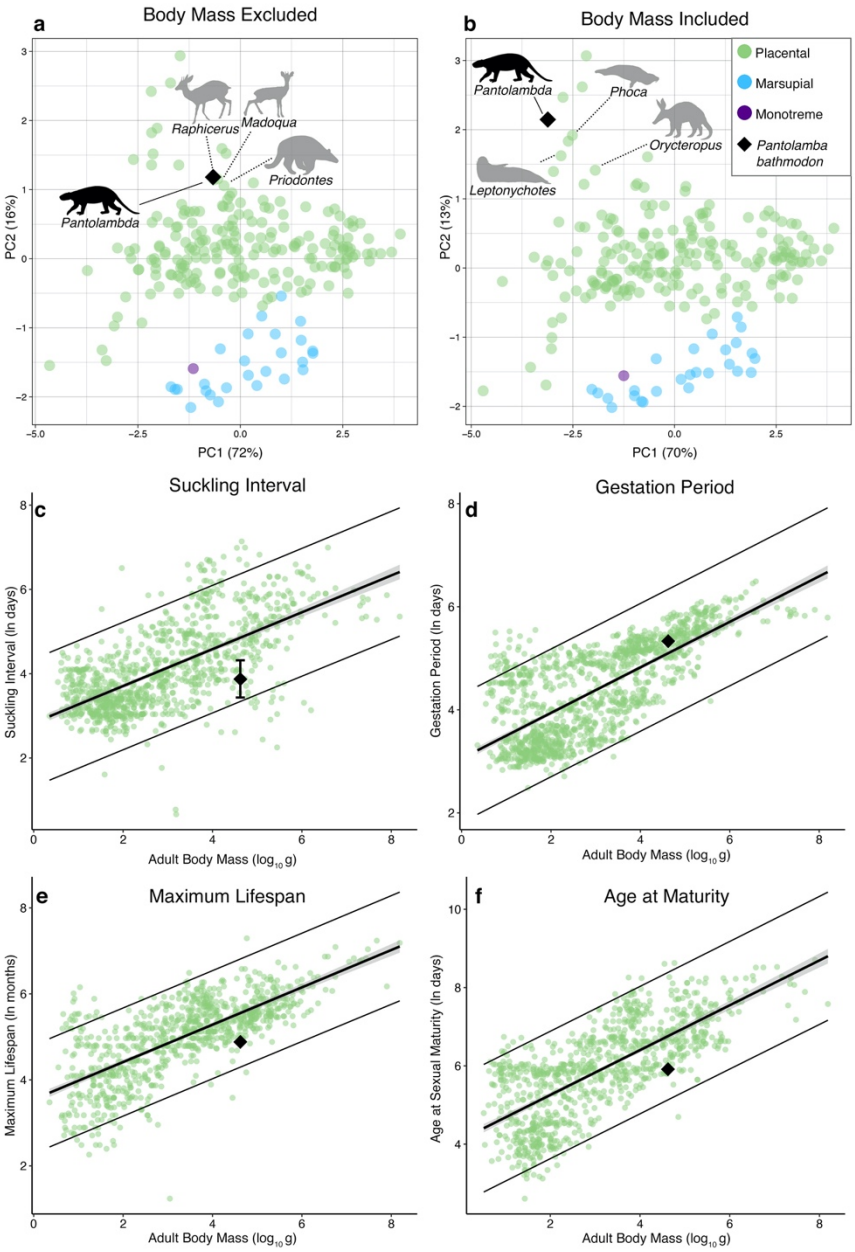

607

608 **Extended Data Fig. 8.** Life history of *P. bathmodon* compared to living mammals. (a, b)
609 principal components analyses using the PanTHERIA dataset (placentals, green; marsupials,
610 blue; monotremes, purple) incorporating suckling interval, gestation period, maximum lifespan,
611 and age at sexual maturity, with adult body mass excluded (a) or included (b) as a variable; close
612 living analogues to *P. bathmodon* indicated by silhouettes. (c–f) regressions of life history
613 variables in placental mammals with 95% confidence intervals (thin black lines) centred on the

generalized linear model regression trendline for suckling interval (c), gestation period (d), maximum lifespan (e), and age at sexual maturity (f), showing that *P. bathmodon* is within the 95% confidence interval of placentals in all parameters. Silhouette of *Pantolambda bathmodon* created by SLS. Silhouettes of *Orycteropus* and *Priodontes* adapted from Phylopic images (CC0 1.0 https://creativecommons.org/publicdomain/zero/1.0/), silhouette of *Leptonychotes* is original artwork by GFF, silhouette of *Phoca* was generated from a photograph taken by GFF, and all others were generated from public domain images (CC0 1.0 https://creativecommons.org/publicdomain/zero/1.0/).

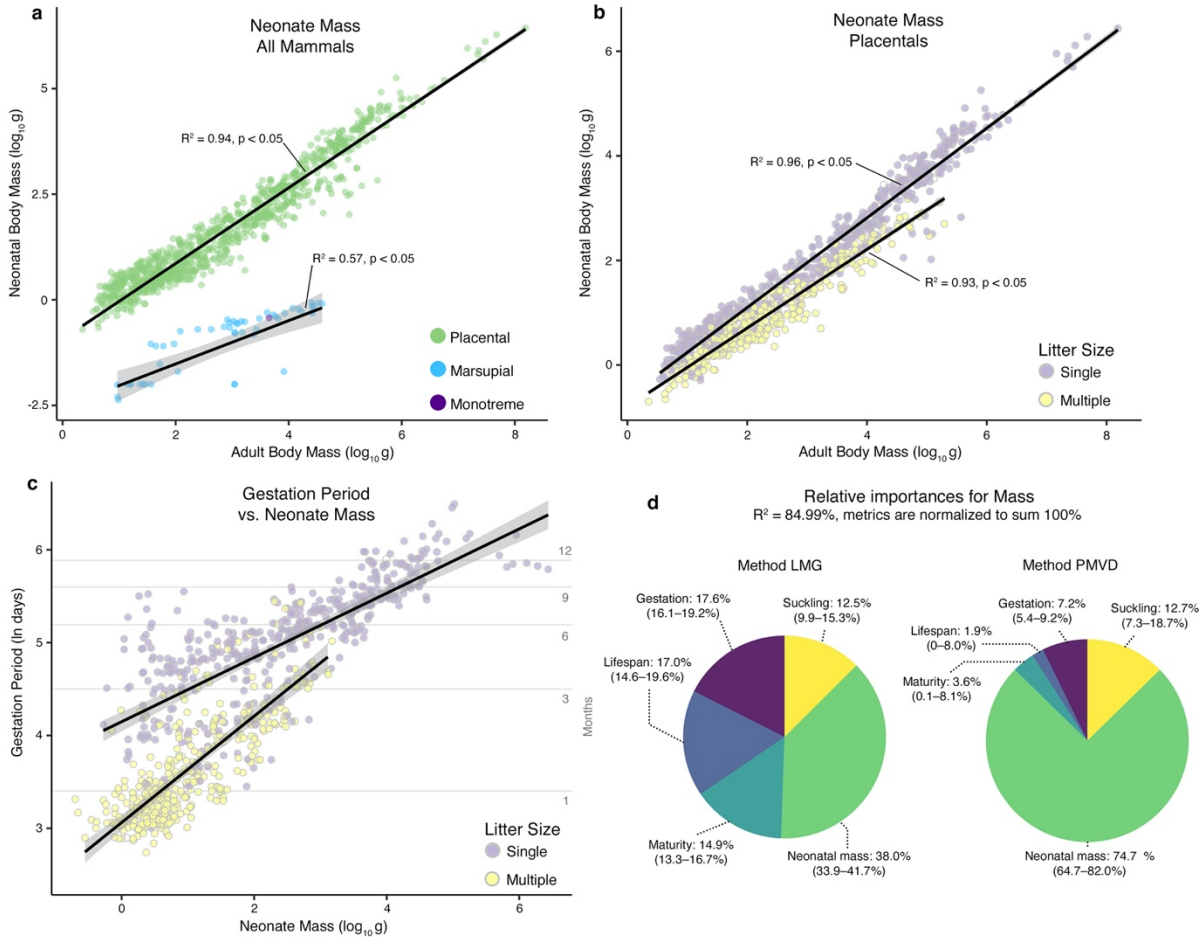

Extended Data Fig. 9. Relationship between neonate mass and adult body mass in extant mammals. (a) Generalized linear model regression of neonate body mass against adult body mass for all species in the PanTheria dataset, showing clear separation of placental mammals (green, p-value < 2.2×10^{-16}) from non-placental mammals (p-value: 4.07×10^{-6}); 95% confidence interval for regression slope shown as shaded envelope. (b) Neonate body mass plotted against adult body mass for placental species, showing tight correlations of neonate mass and adult mass (p values both < 2.2×10^{-16}) ; 95% confidence interval for generalized linear model regression slope shown as shaded envelope. (c) Gestation period plotted against neonate body mass; 95% confidence interval for generalized linear regression slope shown as shaded envelope. (d) Relative importance of multiple regression of adult body mass against neonate weight, gestation period, maximum lifespan, time to sexual maturity, and suckling period, showing relative contribution of factors to adult body mass; confidence intervals derived from 1000 replicates of bootstrapping.

639 **Extended Data Table 1. Quantitative dental histological data for *Pantolambda bathmodon*.**

Specimen (NMMNH)	Element	Retzius Periodicity	Enamel Secretion Rate (μm/d)	Lamination Angle	Crown Extension Rate (μm/d)	Prenatal Formation Time (d)	Crown Formation Time (d)	Cementum Annulations[§]	Trace Element Analysis
P-19541	Lm1	2	9.3	4.4°	93.5	-	154	3	Protoconid
	Lm2	2	9.9[‡]	7.2°	78[‡]	78	195	2.5	Protoconid and Paraconid
P-19612	C	1	9.3	5.0°	89	-	-	3	-
P-19625	M1	1	-	-	-	-	-	5	-
	Root	-	-	-	-	-	-	11*	-
P-22012	P4	-	-	-	-	-	-	7	-
P-27844	LdP2	1	9.2[†]	4.1°	114[†]	116	68	0.5	Paracone
	LdP4	1	-	-	-	-	-	-	Paracone
	LdP5	1	9.75[†]	5.0°	142[†]	138	98	0.5	Protocone
P-41514	LM1	1	-	-	-	-	-	3	-
	LM2	1	-	-	-	-	-	3	-
	LM3	1	-	-	-	-	-	2.5	-
P-69892	Lm3	2	9.1	9.4	71	-	-	2.5	Pilot transect
P-69918	i	1	7.4	6.4°	70	-	121	3	Labial enamel
P-69919	Lp1	1	10.4	6.1°	78	-	115	4	-
P-69923	I	1	7.0	5.65°	49	-	126	4	-
P-69925	C	1	-	-	-	-	-	3	-

640

641 Note: *estimate, see Supplement for further details. For teeth with a neonatal line, [†] prenatal, [‡]

642 postnatal. [§], counted as a pair of light and dark bands; - inapplicable or not available;

643